ACS Macro Letters

pubs.acs.org/macroletters Letter

Tunable Knot Segregation in Copolyelectrolyte Rings Carrying a Neutral Segment

Andrea Tagliabue, Cristian Micheletti,* and Massimo Mella*

Cite This: *ACS Macro Lett.* 2021, 10, 1365−1370 Read Online

ACCESS | Metrics & More | Article Recommendations | Supporting Information

ABSTRACT: We use Langevin dynamics simulations to study the knotting properties of copolyelectrolyte rings carrying neutral segments. We show that by solely tuning the relative length of the neutral and charged blocks, one can achieve different combinations of knot contour position and size. Strikingly, the latter is shown to vary nonmonotonically with the length of the neutral segment; at the same time, the knot switches from being pinned at the block's edge to becoming trapped inside it. Model calculations relate both effects to the competition between two adversarial mechanisms: the energy gain of localizing one or more of the knot's essential crossings on the neutral segment and the entropic cost of such localization. Tuning the length of the neutral segment sets the balance between the two mechanisms and hence the number of localized essential crossings, which in turn modulates the knot's size. This general principle ought to be useful in more complex systems, such as multiblock copolyelectrolytes, to achieve a more granular control of topological constraints.

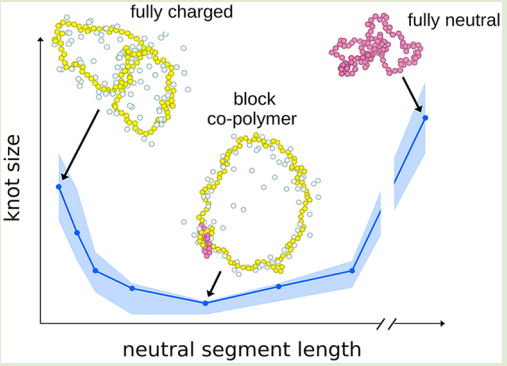

Convergent theoretical and experimental advancements have provided numerous and striking examples of how chain-uncrossability defines an impressive range of polymer properties. Topological constraints can endow linear and circular chains with peculiar relaxation kinetics,[1−8] and metric scaling behavior[9−14] and can affect very distinctively the response of chains to elongational flows,[15−20] mechanical stretching,[21−24] and pore translocation.[25−27]

Nonetheless, we are still far from having an adequate understanding of the multiscale relationship between the global entangled state of polymers and the local structural motifs that ultimately underpin it. For knotted chains, these topology-defining local elements are embodied by the so-called essential crossings. These *loci*, which correspond to localized chain juxtapositions where performing a strand passage alters the chain knotted state, are the gateway to virtually all knotting properties. In fluctuating open chains, the addition or removal of essential crossings at the termini are the primary mechanisms regulating the equilibrium abundance and complexity of knots.[6,28] The intermingling or separation of the prime components of composite knots[29] is arguably relatable to effective interactions between such essential crossings, and so are the stochastic motion of knots along mechanically stretched chains[30] and the long lifetimes of tangles in supercoiled knotted DNA.[31,32]

Achieving even partial external control of the essential crossings can open new theoretical and applicative perspectives, and thus, it is of primary interest to identify polymer systems that are best suited to this endeavor.

Here we consider a class of copolyelectrolyte (co-PE) rings with nontrivial topologies and demonstrate that tuning their composition allows addressing the absolute and relative contour positioning of different subsets of the essential crossings. The co-PEs consist of two segments: one neutral and one charged. We show that by varying their relative lengths it is possible to modulate the effective interactions of the essential crossings and thus tune the contour length and location of the knot in ways that, to our knowledge, have no analog in other polymeric systems. In particular, we show that the knot size has a striking nonmonotonic dependence on the ring composition, as it has with respect to the polyelectrolyte ionization degree.[33]

The simulated system consists of a knotted block co-PE ring in solution with neutralizing counterions. The bead−spring ring has either a 3_1 or a 5_1 topology and is made of $N = 120$ monomers of which N_{neu} forms the neutral segment (NS) and the rest carry a monovalent negative charge (see Figure 1). The ring is simulated in a periodic cubic simulation cell of side $L = 76\sigma$, along with $N - N_{neu}$ positive monovalent counterions. All particles have a nominal diameter σ, and a WCA potential[34] is used for their steric interactions. Charged particles

Received: July 11, 2021
Accepted: September 13, 2021
Published: October 19, 2021

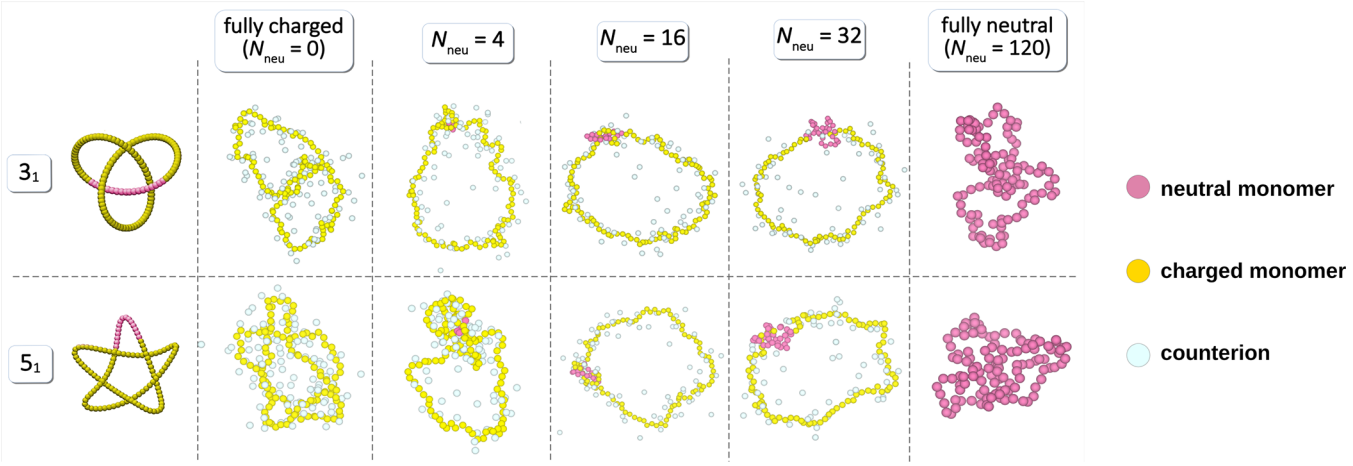

Figure 1. Typical configurations of knotted co-PE rings and surrounding counterions. The rings consist of N_{mono} = 120 monomers, of which N_{neu} form the NS and the others are charged, see legend. The configurations for other values of N_{neu} are shown in Figure S1.

additionally interact via a Coulomb potential, with Bjerrum length $l_B = 2\sigma$, and ring connectivity is provided by a FENE term.[35] For a typical monomer size of σ = 3.55 Å, the settings correspond to a 10 mM monomer concentration and to l_B = 7.10 Å, as appropriate for dilute aqueous solutions at room temperature. N_{neu} varies in the 2−32 range, with also N_{neu} = 0 (fully charged polyelectrolyte) and $N_{neu} = N$ = 120 (neutral ring) cases simulated for reference. For each value, we collected 100 independent Langevin dynamics trajectories with the software package ESPResSo.[36] The knotted region was located with the KymoKnot package,[37] which implements a bottom-up search of the shortest arc that, after suitable closure, has the same topology of the entire ring. Unlike the knotted state of the entire ring, which is well-defined topologically, the knotted state of an open arc depends on the closure scheme and, hence, on geometry. We adopted the minimally invasive closure scheme, which bridges the arc's termini either directly or via the convex hull, depending on the shortest route.[38] Additional model and setup details are provided as Supporting Information (SI).

A first overview of the results is given in Figure 1, which shows typical configurations of the knotted rings for different N_{neu} values. As the latter increases from zero, two different phenomena occur: (i) the knotted region becomes pinned at the NS and (ii) the knot goes from completely delocalized to strongly localized and, eventually, back to a less localized state.

These two effects are illustrated in Figure 2. Figure 2a portrays the probability p that the 3_1 or 5_1 knotted regions contain one or more neutral monomers. The p curves rise steeply, with N_{neu} remaining well above the reference curves for uniform contour positioning (p^0), thus, indicating the significance of the increased likelihood of the knotted region to be part of the NS. In fact, for $N_{neu} \geq 16$, knots are almost exclusively found in correspondence of the NS for both topologies.

Figure 2b presents, instead, the N_{neu} dependence of the average length of the knotted regions, $\langle l_K \rangle$. Strikingly, the curves have a nonmonotonic behavior, with minima at N_{neu} = 16 and 24 for the 3_1 and 5_1 topologies, respectively. In both cases, the corresponding knot length is about 40% of the value for fully charged rings (N_{neu} = 0), thus, denoting tight knotted states, see Figure 1. Further increasing N_{neu} causes knots to steadily grow in size toward the fully neutral ring limit (N_{neu} = 120), where they become again delocalized with $\langle l_K \rangle \approx 61$ and 80 for 3_1 and 5_1 topologies, respectively. The corresponding l_K distributions are provided in Figure S2.

The fact that the two delocalized limits for the fully neutral and charged co-PEs are bridged nonmonotonically is unexpected, and so it is the fact that tighter knotted states exist in between. Both the existence of a minimum in the $\langle l_K \rangle$ curves, and the pinning of knots in correspondence of even very short NSs, are properties that cannot be predicted nor accounted for by available models of polymer knotting, including flexible/rigid block copolymers[39] that we discuss further below. In the following, we thus examine and discuss the microscopic origin of such effects and their broader implications.

As a first step, we analyze how the contour location of the knotted portion relative to the NS varies with N_{neu}. The results for N_{neu} = 4, 16, and 32, are shown in Figure 3, where the $\rho(\delta_{NS})$ curves portray the probability density that the knotted portion includes monomers at a contour distance δ_{NS} from the two NS midpoint, see also SI. The companion probability distributions ρ_{mid} correspond, instead, to the location of the knot midpoint.

For the 3_1 knot (Figure 3a−c), ρ presents a maximum at the center of the NS (i.e., $\delta_{NS} = 0$) for all the N_{neu} values. For short NS (e.g., N_{neu} = 4) the probability distribution has a plateau that extends significantly into the charged segment and dies off at $\delta_{NS} \approx 30$. The knot midpoint is preferentially located at the center of the plateau region and is hardly found inside the NS. Considering that $\langle l_K \rangle \approx 25$, the result indicates that very short NSs suffice to pin the knot, but the pinning only occurs at the very edge of the knotted region. Instead, at N_{neu} = 16, which yields the minimum length of the 3_1 knot, the protrusion of ρ into the charged segment is limited to fewer than 10 monomers, and the most probable location of the knot midpoint about coincides with the NS center. Thus, the knot is not only pinned at the NS, but it is mostly contained inside it. Finally, at N_{neu} = 32, the knotted region is solidly contained within the NS and centered at its midpoint.

These properties differ in several ways from those of the 3_1-knotted flexible/rigid block copolymers at low temperature. In such systems, knots are preferentially located in flexible regions, but when the latter are very short, other favored positions exist in the region, too. In addition, delocalized knots

https://doi.org/10.1021/acsmacrolett.1c00453
ACS Macro Lett. 2021, 10, 1365−1370

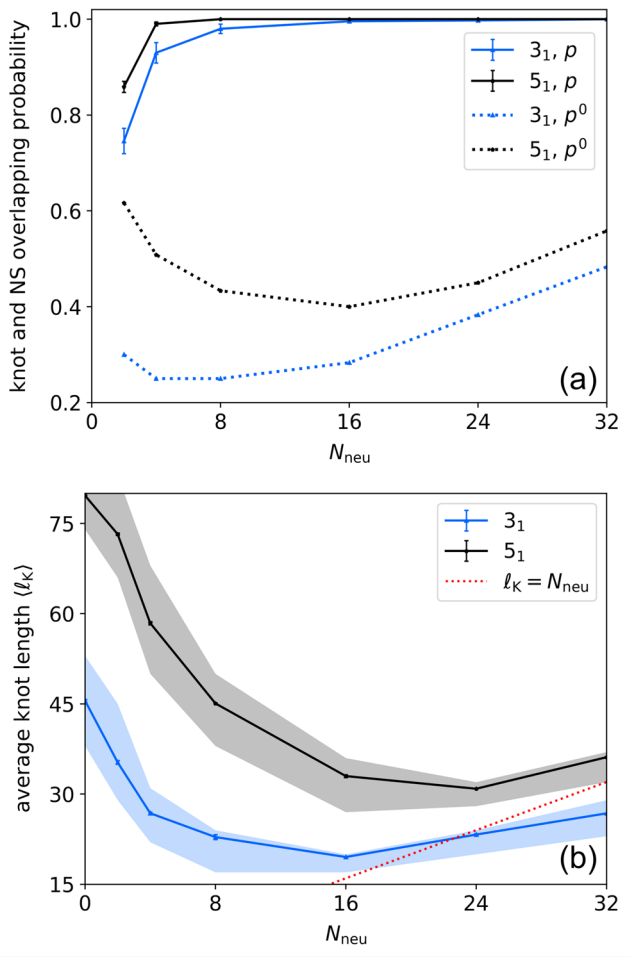

Figure 2. (a) Probability, p, that one or more neutral monomers are included in the 3_1- and 5_1-knotted regions. The data are shown for varying lengths of the NS, N_{neu}. They are compared with the analogous probability for the null reference case, where the knotted region has a uniform probability of being anywhere on the ring, $p^0 = (N_{neu} + (\mathrm{int}\langle l_K\rangle - 1))/N$. $\langle l_K\rangle$ is the average length of the knotted region (measured in the number of monomers, see the SI), and its dependence on N_{neu} is shown in panel (b) for both considered topologies. The edges of the thick bands mark the 25th and 75th percentiles of the knot length distributions (reported in Figure S2). The $\langle l_K\rangle = N_{neu}$ line is shown for reference.

are repelled by flexible segments that are somewhat smaller than the typical knot size.[39] Such competing effects were not observed in our block copolyelectrolytes, where knots are solely attracted to the NS, regardless of its size.

The 5_1 topology (Figure 3d–f) presents similar trends of increasing pinning and localization inside growing NSs, but with two noticeable differences from the 3_1 case. First, the support of ρ is systematically broader due to the more complex topology. Second, ρ_{mid} has two maxima at intermediate values of N_{neu}, the two modal locations corresponding to the edges of the NS and its midpoint.

The kinetic counterparts of the pinning and localization effects are illustrated by the trajectories reported in the insets of Figure 3; these represent the contour motion of the knot midpoint. For small N_{neu} values, the midpoint stays close to one or the other edge of the NS, remaining at a distance about equal to $l_K/2$, and only rarely move through the NS. As the NS grows, knot sliding across it becomes more likely, as shown in Figure 3e for $N_{neu} \approx 16$. Note that for the more complex 5_1 topology, the knot midpoint can not only cross the NS, but can stay temporarily pinned at specific locations inside it; see the blue trajectory in the inset of Figure 3e. These alternate preferential positionings reflect in the noticeable multimodality of the ρ_{mid} profile and have no counterpart for the 3_1-knot case. Finally, at sufficiently large N_{neu} values, the knot midpoint trajectories once entering the NS become persistently trapped inside it. In this case, the restricted motion inside the NS appears to be mostly stochastic, without noticeable pinning at specific locations.

To clarify the microscopic origin of this unexpectedly complex behavior, we introduce an interpretative framework based on energy calculations performed by keeping fixed the conformation of the knotted ring while sliding the NS along the chain contour. With this approach, we are thus able to profile the electrostatic energy (for simplicity, computed in the absence of counterions) and to establish the energy-minimizing positions of the NS for different choices of l_K. The model calculations thus allow for addressing the interplay of the knotted region and the NS from a complementary perspective with respect to the Langevin trajectories in which it is the shape of the knotted ring that adjusts for the co-PEs composition to be in canonical equilibrium.

Figure 4a shows the Coulomb energy profiles for a 3_1-knotted ring with $l_K = 32$ at various N_{neu} values. The energy curves are shown as a function of the contour distance, δ_K, between the knot and the NS midpoints (see Figure 4b). For $N_{neu} = 4$, the global minimum is found at $\delta_K^{(min)} = 15$, and a second minimum around $\delta_K^{(min)} = 0$. For $N_{neu} = 16$, we found two (almost equivalent) minima around $\delta_K^{(min)} = 0$ and 11. Finally, for $N_{neu} = 32$, $\delta_K^{(min)} \approx 10$. Analogous plots for different knot sizes and 5_1 knots are given in Figure S3.

The implications are aptly conveyed by the accompanying 1D representations of the rings, where the knotted region is marked together with the three pairs of loci corresponding to the essential crossings (Figure 4c). These correspond to pairs of loci that are forced to be nearby by the topological constraints and thus were conveniently identified as the sites for which the global curvature[40] is minimum (see Figure S6).

For small N_{neu}, one observes that the lowest energy is attained when the NS covers either one or two of the peripheral essential crossings. The result is consistent with the intuition that essential crossings, for the proximity of the intervening strands, contribute significantly to the overall electrostatic repulsion of the ring. Thus, the Coulomb energy of the entire system can be significantly lowered by placing even a very short NS in correspondence of the proximal locus of one essential crossing.

As clarified by the energy profile of Figure 4a, the energy reduction is maximum for the outermost essential crossing. This remains the case as N_{neu} is increased up to about $l_K/3$. Beyond such a length, the NS becomes long enough to cover the proximal loci of two essential crossings, which further lowers the overall electrostatic energy of the system. Eventually, when $N_{neu} \geq l_K/2$, the NS is sufficiently long to cover the loci of all three essential crossings, yielding an optimal reduction of the electrostatic repulsion. Upon increasing N_{neu}, the accompanying potential energy minimum becomes progressively broader and shallower as more NS positioning spanning all crossings becomes available, see also Figure S4. Analogous considerations apply to the 5_1 topology, with the proviso that the more numerous essential crossings

https://doi.org/10.1021/acsmacrolett.1c00453
ACS Macro Lett. 2021, 10, 1365−1370

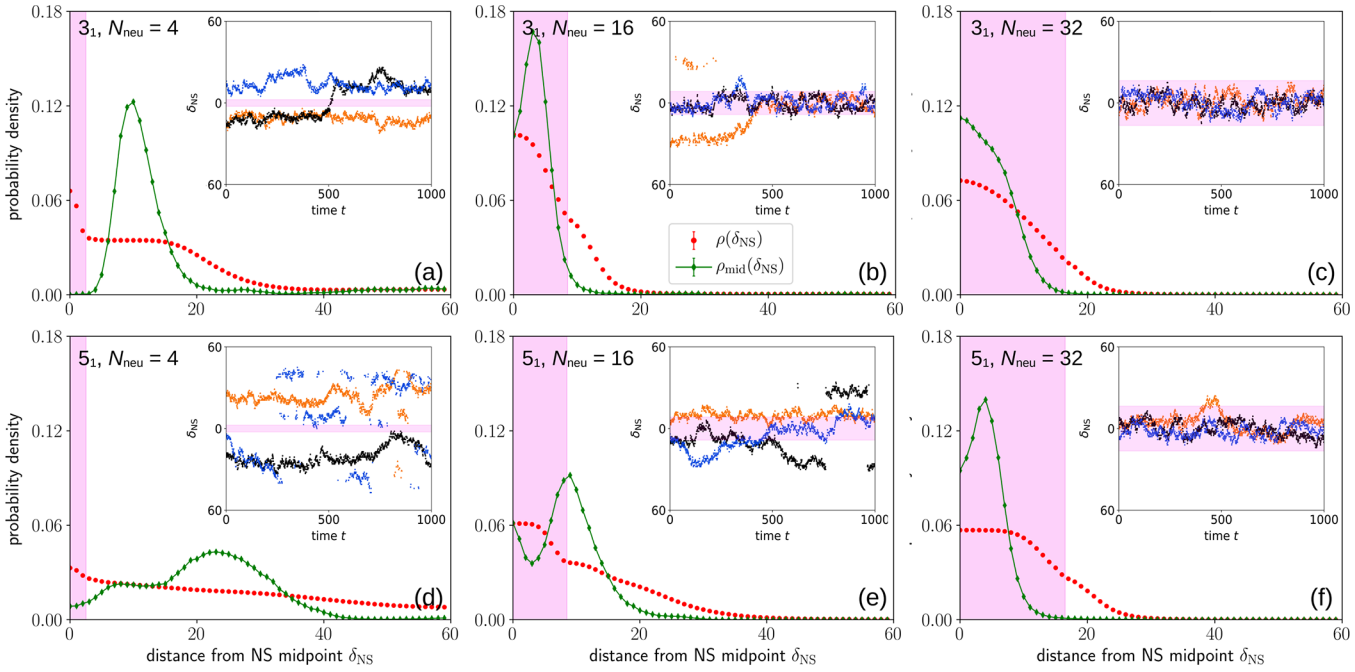

Figure 3. For each value of N_{neu}, we report the probability distribution, $\rho(\delta_{NS})$, that the knotted region includes monomers at a sequence distance δ_{NS} from the NS midpoint. $\rho_{mid}(\delta_{NS})$ is, instead, the probability distribution that the knot midpoint is at distance δ_{NS}. Typical time evolution of the knot midpoints is shown in the insets (time expressed in τ_{MD} units, see the SI). Analogous plots for additional values of N_{neu} are shown in Figure S3.

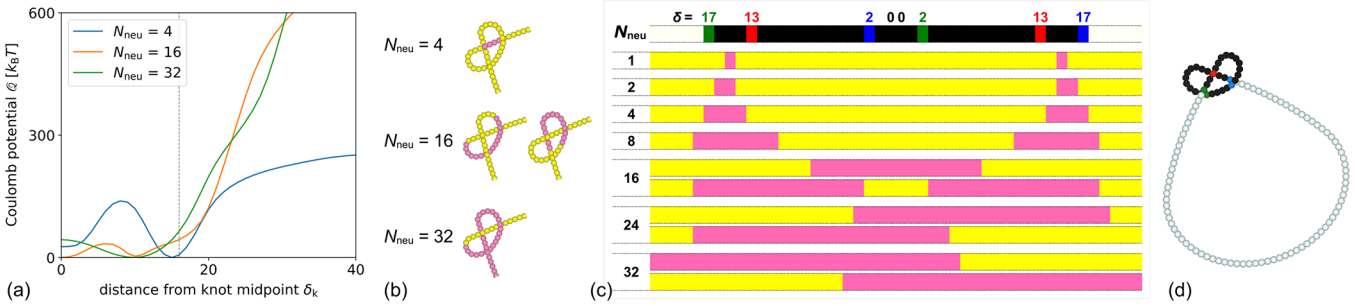

Figure 4. (a) Profile of the Coulomb energy, Q, of a model 3_1-knotted ring (shown in panel d) for different NS lengths, N_{neu}; for the sake of comparison, Q values have been shifted so that the minimum value is zero. (b) Energy-minimizing conformations. (c) One-dimensional, sequence-wise representations of the knot contour indexed by δ_K, that is, the sequence distance of the NS midpoint from the center of the knot; distinct blocks for the same N_{neu} value correspond to symmetric, or otherwise degenerate, energy-minimizing positions. Monomers defining the three essential crossings are highlighted with different colors in panels (c) and (d).

create opportunities for pinning short NSs not only at the edge of the knotted regions, but also inside it (see Figure S5).

The latter results are directly transferable to the more complex case of fluctuating rings, as illustrated in Figure 5 for 3_1-knotted co-PEs and N_{neu} = 4 and 32; see panels (a) and (b), respectively (see also Figures S7 and S8 for other N_{neu} values and the 5_1 case). For each sampled knot size l_K, the heatmaps show how the magnitude of the mean effective unsigned charge of monomers varies with the distance from the knot midpoint. The side plots show, instead, the corresponding probability distribution of l_K. For N_{neu} = 4 (panel a), one clearly notes a colored band running parallel and close to the diagonal, marking the knot boundary. The band corresponds to a small average charge of the monomers and thus reflects the tendency of short NSs to lean against the knot boundary. Such positioning allows the neutral block to cover the outermost locus of the essential crossings, in full analogy with the energy-minimizing solution of the rigid-ring model. As N_{neu} increases, the band increases its width (e.g., see panel b), remaining close and parallel to the diagonal.

An important difference with the rigid-ring model is that, in fluctuating co-PEs, both the positioning and the size of the knotted region are co-opted to lower the system free energy. Thus, the nonmonotonic $\langle l_K \rangle$ curve in Figure 2b is explained by the fact that minimizing the repulsion of essential crossings is so energetically advantageous that the knotted region tightens as much as entropic penalties consent so to maximize its coverage by the NS.

In summary, we considered knotted block co-PE rings in solution with counterions and demonstrated that tuning the ring composition allows for varying the contour positioning and size of the knotted region. Even a short NS suffices to pin the knotted region at one of its edges and hinder the knot motion across it. Strikingly, while the knot trapping effect increases with the size of the NS, the length of the knotted region varies nonmonotonically with the rings' composition.

https://doi.org/10.1021/acsmacrolett.1c00453
ACS Macro Lett. 2021, 10, 1365−1370

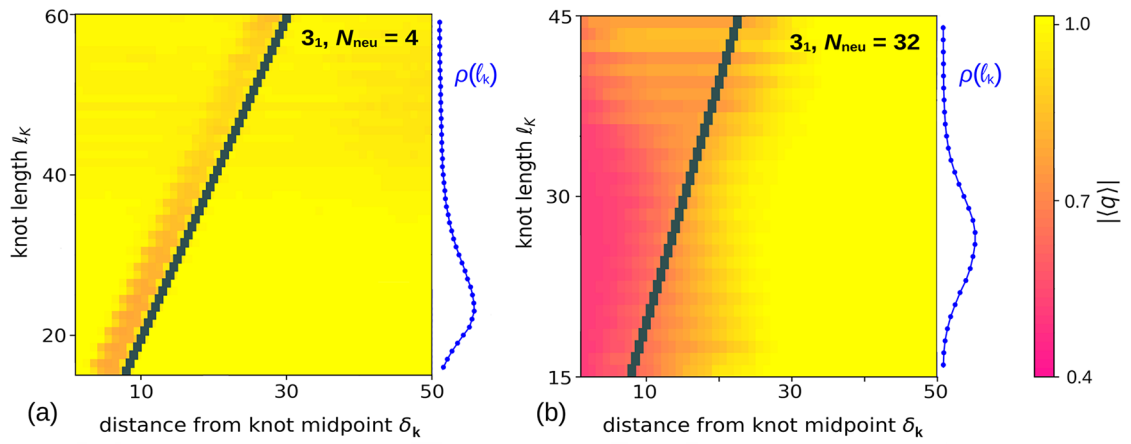

Figure 5. Unsigned average effective charge $|\langle q \rangle|$ of monomers in 3_1-knotted rings with the indicated lengths of the NS, N_{neu}. The average is taken at various knot lengths (l_K, y axis) and sequence distances (δ_K, x axis) from the knot midpoint. For reference, the $l_K = 2\delta_K$ line is superposed to the main graphs, and the side plots are the normalized knot length probability distributions $\rho(l_K)$, see also Figure S2.

By using model calculations, we showed that all of these properties originate from the lower Coulomb energy of states with essential crossings in the NS. Minimizing the system's free energy thus involves balancing this energy gain, which promotes the localization of all essential crossings in the NS, with the entropic cost of such localization. The relative weight of the two adversarial terms can be controlled by the size of the NS. Different combinations of pinning degree and size of the knotted regions can thus be realized with a judicious design of the rings' composition.

We expect that the knotting properties and design principles discussed here ought to be relevant for systems such as PEG-*b*-PEI rings, which are easily quaternized, as well as being applicable to more general contexts. For example, co-PEs with multiple alternating charged and neutral blocks represent a natural extension of the baseline diblock form considered here, which should afford a more granular determination of the absolute and relative positioning of essential crossings. These systems could also be used to probe the effective interactions between essential crossings that, despite being central to the understanding of knotted polymers, have been considered only recently;[30] alternatively, they could be investigated for the possible segregation of the prime components in composite knots. Short-ranged attractive interactions, such as the ones mediated by coordinating counterions, also represent a promising avenue for the possibility to localize the knot essential crossings in the charged region.[41]

Other relevant physical properties could be tuned along with chemical composition to influence the barriers for pinning or localizing knots, such as the total contour length of the ring,[42] the background ionic strength[33] of the solution, or the solvent quality. Besides, intrinsically short-ranged attraction in a neutral block (e.g., the ones due to a limited solvophilicity or the ability to form intrachain chemical specific interactions[43,44]), may strengthen or even induce[41] the tendency to knot pinning, provided the NS is sufficiently long to position a few of its monomers in the regions facing each other in an essential crossing.

■ ASSOCIATED CONTENT

Supporting Information

The Supporting Information is available free of charge at https://pubs.acs.org/doi/10.1021/acsmacrolett.1c00453.

Model and methods: simulation protocol and knot analysis; Results; References (PDF)

■ AUTHOR INFORMATION

Corresponding Authors

Cristian Micheletti − *SISSA (Scuola Internazionale Superiore di Studi Avanzati), 34136 Trieste, Italy;* orcid.org/0000-0002-1022-1638; Email: cristian.micheletti@sissa.it

Massimo Mella − *Dipartimento di Scienza ed Alta Tecnologia, Universitá degli Studi dell'Insubria, 22100 Como, Italy;* orcid.org/0000-0001-7227-9715; Email: massimo.mella@uninsubria.it

Author

Andrea Tagliabue − *Dipartimento di Scienza ed Alta Tecnologia, Universitá degli Studi dell'Insubria, 22100 Como, Italy;* orcid.org/0000-0001-9520-0627

Complete contact information is available at: https://pubs.acs.org/10.1021/acsmacrolett.1c00453

Notes

The authors declare no competing financial interest.

■ ACKNOWLEDGMENTS

M.M. acknowledges funding from the Universit degli Studi dell'Insubria (Fondo d'Ateneo per la Ricerca, FAR2020). A.T. thanks the Universit degli Studi dell'Insubria for a Ph.D. studentship.

■ REFERENCES

(1) Everaers, R.; Sukumaran, S. K.; Grest, G. S.; Svaneborg, C.; Sivasubramanian, A.; Kremer, K. Rheology and microscopic topology of entangled polymeric liquids. *Science* **2004**, *303*, 823−826.

(2) Tzoumanekas, C.; Theodorou, D. N. Topological analysis of linear polymer melts: a statistical approach. *Macromolecules* **2006**, *39*, 4592−4604.

(3) Rosa, A.; Everaers, R. Structure and dynamics of interphase chromosomes. *PLoS Comput. Biol.* **2008**, *4*, e1000153.

(4) Tang, J.; Du, N.; Doyle, P. S. Compression and self-entanglement of single DNA molecules under uniform electric field. *Proc. Natl. Acad. Sci. U. S. A.* **2011**, *108*, 16153−16158.

(5) Micheletti, C.; Orlandini, E. Knotting and unknotting dynamics of DNA strands in nanochannels. *ACS Macro Lett.* **2014**, *3*, 876−880.

(6) Amin, S.; Khorshid, A.; Zeng, L.; Zimny, P.; Reisner, W. A nanofluidic knot factory based on compression of single DNA in nanochannels. *Nat. Commun.* **2018**, *9*, 1−10.
(7) Michieletto, D.; Orlandini, E.; Turner, M. S.; Micheletti, C. Separation of Geometrical and Topological Entanglement in Confined Polymers Driven out of Equilibrium. *ACS Macro Lett.* **2020**, *9*, 1081−1085.
(8) Smrek, J.; Chubak, I.; Likos, C. N.; Kremer, K. Active topological glass. *Nat. Commun.* **2020**, *11*, 1−11.
(9) Grosberg, A.; Rabin, Y.; Havlin, S.; Neer, A. Crumpled globule model of the three-dimensional structure of DNA. *EPL (Europhysics Letters)* **1993**, *23*, 373.
(10) Virnau, P.; Kantor, Y.; Kardar, M. Knots in Globule and Coil Phases of a Model Polyethylene. *J. Am. Chem. Soc.* **2005**, *127*, 15102−15106.
(11) Ercolini, E.; Valle, F.; Adamcik, J.; Witz, G.; Metzler, R.; De Los Rios, P.; Roca, J.; Dietler, G. Fractal dimension and localization of DNA knots. *Phys. Rev. Lett.* **2007**, *98*, 058102.
(12) Deguchi, T.; Uehara, E. Statistical and dynamical properties of topological polymers with graphs and ring polymers with knots. *Polymers* **2017**, *9*, 252.
(13) Amici, G.; Caraglio, M.; Orlandini, E.; Micheletti, C. Topologically Linked Chains in Confinement. *ACS Macro Lett.* **2019**, *8*, 442−446.
(14) Zhang, J.; Meyer, H.; Virnau, P.; Daoulas, K. C. Can Soft Models Describe Polymer Knots? *Macromolecules* **2020**, *53*, 10475−10486.
(15) Metzler, R.; Reisner, W.; Riehn, R.; Austin, R.; Tegenfeldt, J.; Sokolov, I. M. Diffusion mechanisms of localised knots along a polymer. *EPL (Europhysics Letters)* **2006**, *76*, 696.
(16) Renner, C. B.; Doyle, P. S. Stretching self-entangled DNA molecules in elongational fields. *Soft Matter* **2015**, *11*, 3105−3114.
(17) Liebetreu, M.; Ripoll, M.; Likos, C. N. Trefoil Knot Hydrodynamic Delocalization on Sheared Ring Polymers. *ACS Macro Lett.* **2018**, *7*, 447−452.
(18) Ma, Z.; Dorfman, K. D. Diffusion of Knots along DNA Confined in Nanochannels. *Macromolecules* **2020**, *53*, 6461−6468.
(19) Soh, B. W.; Doyle, P. S. Deformation Response of Catenated DNA Networks in a Planar Elongational Field. *ACS Macro Lett.* **2020**, *9*, 944−949.
(20) Liebetreu, M.; Likos, C. N. Hydrodynamic inflation of ring polymers under shear. *Commun. Mater.* **2020**, *1*, 1−11.
(21) Bao, X. R.; Lee, H. J.; Quake, S. R. Behavior of complex knots in single DNA molecules. *Phys. Rev. Lett.* **2003**, *91*, 265506.
(22) Farago, O.; Kantor, Y.; Kardar, M. Pulling knotted polymers. *Europhys. Lett.* **2002**, *60*, 53−59.
(23) Huang, L.; Makarov, D. E. Langevin Dynamics Simulations of the Diffusion of Molecular Knots in Tensioned Polymer Chains. *J. Phys. Chem. A* **2007**, *111*, 10338−10344.
(24) Caraglio, M.; Micheletti, C.; Orlandini, E. Stretching Response of Knotted and Unknotted Polymer Chains. *Phys. Rev. Lett.* **2015**, *115*, 188301.
(25) Suma, A.; Rosa, A.; Micheletti, C. Pore translocation of knotted polymer chains: How friction depends on knot complexity. *ACS Macro Lett.* **2015**, *4*, 1420−1424.
(26) Plesa, C.; Verschueren, D.; Pud, S.; Van Der Torre, J.; Ruitenberg, J. W.; Witteveen, M. J.; Jonsson, M. P.; Grosberg, A. Y.; Rabin, Y.; Dekker, C. Direct observation of DNA knots using a solid-state nanopore. *Nat. Nanotechnol.* **2016**, *11*, 1093−1097.
(27) Caraglio, M.; Orlandini, E.; Whittington, S. G. Translocation of links through a pore: effects of link complexity and size. *J. Stat. Mech.: Theory Exp.* **2020**, *2020*, 043203.
(28) Tubiana, L.; Rosa, A.; Fragiacomo, F.; Micheletti, C. Spontaneous knotting and unknotting of flexible linear polymers: Equilibrium and kinetic aspects. *Macromolecules* **2013**, *46*, 3669−3678.
(29) Najafi, S.; Podgornik, R.; Potestio, R.; Tubiana, L. Role of bending energy and knot chirality in knot distribution and their effective interaction along stretched semiflexible polymers. *Polymers* **2016**, *8*, 347.
(30) Caraglio, M.; Marcone, B.; Baldovin, F.; Orlandini, E.; Stella, A. L. Topological disentanglement of linear polymers under tension. *Polymers* **2020**, *12*, 2580.
(31) Buck, G. R.; Zechiedrich, E. L. DNA disentangling by type-2 topoisomerases. *J. Mol. Biol.* **2004**, *340*, 933−939.
(32) Coronel, L.; Suma, A.; Micheletti, C. Dynamics of supercoiled DNA with complex knots: large-scale rearrangements and persistent multi-strand interlocking. *Nucleic Acids Res.* **2018**, *46*, 7533−7541.
(33) Tagliabue, A.; Izzo, L.; Mella, M. Interface Counterion Localization Induces a Switch between Tight and Loose Configurations of Knotted Weak Polyacid Rings despite Intermonomer Coulomb Repulsions. *J. Phys. Chem. B* **2020**, *124*, 2930−2937.
(34) Weeks, J. D.; Chandler, D.; Andersen, H. C. Role of Repulsive Forces in Determining the Equilibrium Structure of Simple Liquids. *J. Chem. Phys.* **1971**, *54*, 5237−5247.
(35) Kremer, K.; Grest, G. S. Dynamics of entangled linear polymer melts: A molecular-dynamics simulation. *J. Chem. Phys.* **1990**, *92*, 5057.
(36) Weik, F.; Weeber, R.; Szuttor, K.; Breitsprecher, K.; de Graaf, J.; Kuron, M.; Landsgesell, J.; Menke, H.; Sean, D.; Holm, C. ESPResSo 4.0 − An Extensible Software Package for Simulating Soft Matter Systems. *Eur. Phys. J.: Spec. Top.* **2019**, *227*, 1789−1816.
(37) Tubiana, L.; Polles, G.; Orlandini, E.; Micheletti, C. KymoKnot: A web server and software package to identify and locate knots in trajectories of linear or circular polymers. *Eur. Phys. J. E: Soft Matter Biol. Phys.* **2018**, *41*, na.
(38) Tubiana, L.; Orlandini, E.; Micheletti, C. Probing the Entanglement and Locating Knots in Ring Polymers: A Comparative Study of Different Arc Closure Schemes. *Prog. Theor. Phys. Suppl.* **2011**, *191*, 192−204.
(39) Orlandini, E.; Baiesi, M.; Zonta, F. How local flexibility affects knot positioning in ring polymers. *Macromolecules* **2016**, *49*, 4656−4662.
(40) Gonzalez, O.; Maddocks, J. H. Global curvature, thickness, and the ideal shapes of knots. *Proc. Natl. Acad. Sci. U. S. A.* **1999**, *96*, 4769−4773.
(41) Dai, L.; Doyle, P. S. Effects of Intrachain Interactions on the Knot Size of a Polymer. *Macromolecules* **2016**, *49*, 7581−7587.
(42) Dommersnes, P. G.; Kantor, Y.; Kardar, M. Knots in charged polymers. *Phys. Rev. E: Stat. Phys., Plasmas, Fluids, Relat. Interdiscip. Top.* **2002**, *66*, 031802.
(43) Tagliabue, A.; Izzo, L.; Mella, M. Absorbed weak polyelectrolytes: Impact of confinement, topology, and chemically specific interactions on ionization, conformation free energy, counterion condensation, and absorption equilibrium. *J. Polym. Sci., Part B: Polym. Phys.* **2019**, *57*, 491−510.
(44) Tagliabue, A.; Izzo, L.; Mella, M. Impact of Charge Correlation, Chain Rigidity, and Chemical Specific Interactions on the Behavior of Weak Polyelectrolytes in Solution. *J. Phys. Chem. B* **2019**, *123*, 8872−8888.

https://doi.org/10.1021/acsmacrolett.1c00453
ACS Macro Lett. 2021, 10, 1365−1370